Transient ballistic and diffusive phonon heat transport in thin films

A. A. Joshi and A. Majumdar

Citation: Journal of Applied Physics **74**, 31 (1993); doi: 10.1063/1.354111
View online: http://dx.doi.org/10.1063/1.354111
View Table of Contents: http://scitation.aip.org/content/aip/journal/jap/74/1?ver=pdfcov
Published by the AIP Publishing

Transient ballistic and diffusive phonon heat transport in thin films

A. A. Joshi and A. Majumdar
Department of Mechanical and Environmental Engineering, University of California, Santa Barbara, California 93106

(Received 20 January 1993; accepted for publication 17 March 1993)

Ballistic and diffusive phonon transport under small time and spatial scales are important in fast-switching electronic devices and pulsed-laser processing of materials. The Fourier law represents only diffusive transport and yields an infinite speed for heat waves. Although the hyperbolic heat equation involves a finite heat wave speed, it cannot model ballistic phonon transport in short spatial scales, which under steady state follows the Casimir limit of phonon radiation. An equation of phonon radiative transfer (EPRT) is developed which shows the correct limiting behavior for both purely ballistic and diffusive transport. The solution of the EPRT for diamond thin films not only produces wall temperature jumps under ballistic transport but shows markedly different transient response from that of the Fourier law and the hyperbolic heat equation even for predominantly diffusive transport. For sudden temperature rise at one film boundary, the results show that the Fourier law and the hyperbolic heat equation can significantly over- or underpredict the boundary heat flux at time scales smaller than the phonon relaxation times.

I. INTRODUCTION

Heat transport in dielectric materials and semiconductors is predominantly by phonons, which are quanta of crystal vibrational energy. Transient heat transport by phonons is of vital importance in several technological applications. For example, microelectronics devices are composed mainly of thin films of semiconductors such as Si or GaAs, of dielectrics such as SiO_2 and Si_3N_4, and of metals. The reduction of device sizes to the submicrometer range not only increases the device switching speed to the nanosecond and picosecond range[1] but also increases the local rate of heat generation due to electron-phonon interactions. This leads to very high transient thermal loads on a device. To enhance heat dissipation, new and future devices are likely to contain thin films of high-thermal-conductivity dielectric materials such as diamond and AlN. To predict the performance of electronic devices, it is important to understand the transient thermal behavior of semiconductors and dielectric thin films. Transient heat transport is also critical in pulsed-laser processing of materials,[2] where rapid heating of a material is caused due to incidence of high-power lasers with pulses in the nanosecond range. This can raise the temperature locally above a phase-transition temperature for a very short duration. Since both the temperature as well as the rate of heating and cooling determine the microstructure of the material,[3] it is important to understand the mechanisms of transient phonon transport in order to obtain the desired microstructure.

In the above applications, it is important to note that heat transport must be considered under both short time and spatial scales. This can seldom be analyzed by macroscopic laws of heat transport. First consider the effect of only small spatial scales on steady-state heat transport. When the size of an object is much larger than the phonon mean free path, heat transport is purely diffusive and is accurately modeled by the Fourier law

$$\mathbf{q}=-\lambda\nabla T, \tag{1}$$

where $\mathbf{q}$ is the heat flux vector, λ is the thermal conductivity, and T is the temperature. Based on kinetic theory, the thermal conductivity can be related to other physical properties as[4]

$$\lambda=\tfrac{1}{3}Cvl, \tag{2}$$

where C is the volumetric heat capacity, v is the average speed of sound, and l is the phonon mean free path. However, when the phonon mean free path is of the order of or larger than the medium size, the Fourier law breaks down since the transport is not purely diffusive and is partly ballistic. In this case, a temperature gradient cannot be established within the medium. In the limit of purely ballistic transport and when the temperatures are much lower than the Debye temperature, the heat flux is governed by the Casimir[5] limit given as

$$q=\sigma(T_1^4-T_2^4). \tag{3}$$

This is analogous to photon radiation in an optically thin medium[6] where σ is the Stefan–Boltzmann constant for phonons. Using Monte Carlo simulations, Klitsner *et al.*[7] have shown that in this ballistic limit, temperature jumps occur at the walls of the medium and the heat flux does follow the Casimir limit. As the mean free path is reduced, the wall temperature jumps decrease until, in the macroscopic limit, they become negligible. This is qualitatively shown in Fig. 1. In another approach, Majumdar[8] used the Boltzmann transport equation to derive an equation of phonon radiative transfer (EPRT) similar to the one used to analyze photon radiative transfer in scattering and absorbing media.[6,9] The solution to this equation yielded both the limiting cases of Casimir limit for purely ballistic transport and the Fourier limit for purely diffusive transport. In the intermediate range, the predictions were in excellent agreement with those of Klitsner *et al.*[7] Therefore in the

 0021-8979/93/74(1)/31/9/$6.00

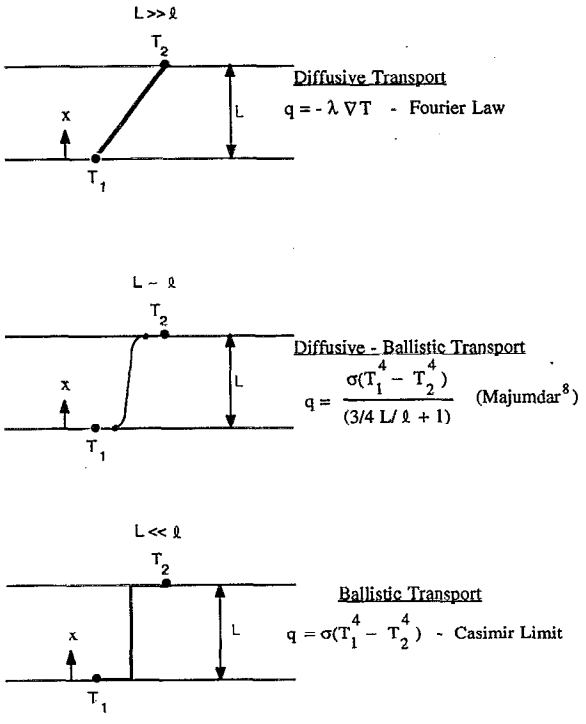

FIG. 1. Schematic diagram qualitatively showing the steady-state temperature profiles under diffusive and ballistic phonon transport.

phonon ballistic transport regime, the Fourier law cannot be used and one must resort to either Monte Carlo simulations or solving the EPRT.

Second, consider the effect of short time scales of the order of the phonon relaxation times on heat transport. It can be argued that the Fourier law cannot be used for this case since the heat equation suggests an infinite speed of heat propagation. Instead, the hyperbolic heat equation is often used to obtain a wavelike solution, where heat waves have a finite propagation speed. The basis of the hyperbolic heat equation is the Cattaneo equation[10] given as

$$\tau_R \frac{\partial q}{\partial t} + q = -\lambda \nabla T, \tag{4}$$

where τ_R is the effective relaxation time given by l/v and l is the effective mean free path and v is the velocity of phonons. Since this also assumes a temperature gradient in the medium, it does not address the ballistic nature of phonon transport. Therefore, although the hyperbolic heat equation may be a good model for short time scales, it cannot be used for short spatial scales. This was analytically shown by Majumdar[8] where the Cattaneo equation was derived from the EPRT only in the purely diffusion limit.

It is clear from the above discussion that for analyzing transient heat transport in the ballistic regime, the classical Fourier law and the hyperbolic heat equation cannot be used. Claro and Mahan[11] analyzed phonon transport for steep temperature gradients within a mean free path and showed that heat conduction is slower than the classical theories predict. They, however, do not predict any temperature jumps under ballistic transport as demonstrated by both the Monte Carlo simulations and the EPRT. In this article, the transient EPRT is used to analyze heat transport under both short time and spatial scales. The results are compared with those obtained from the Fourier law and the hyperbolic heat equation to demonstrate the differences in the predictions and the errors that one might make if the classical laws are used.

II. THEORY

The theory developed in this section can be applied to any medium where phonon heat transport is the dominant mode. Consider a dielectric film of thickness L, initially at temperature T_0. At time $t=0$, the temperature at $x=0$ is increased to T_1 while the temperature at $x=L$ is maintained at T_0, as schematically shown in Fig. 1. Such a situation arises when a dielectric film is sandwiched between two metallic films. Since the electron-phonon mean free path in metals is much smaller than the phonon mean free path in the dielectric film, the two interfaces can be assumed to be thermalizing black boundaries at fixed temperatures. The following dimensionless variables are defined:

$$\theta=\frac{T-T_0}{T_1-T_0}, \quad \xi=\frac{x}{L}, \quad \tau=\frac{t}{(L/v)}, \quad \eta_L=\frac{L}{l}. \tag{5}$$

Here, η_L is defined as the acoustical thickness of the medium explained further in Sec. III. The transient heat transport predicted by the Fourier law, the hyperbolic heat equation, and the EPRT are now studied.

A. Fourier law

In the Fourier law or diffusion limit, the transient energy equation can be written as

$$\frac{\partial T}{\partial t}=\alpha \frac{\partial^2 T}{\partial x^2}, \tag{6}$$

with boundary conditions

$$\text{at } t=0,\ T=T_0, \quad \text{at } x=0,\ T=T_1, \quad \text{at } x=L,\ T=T_0. \tag{7}$$

Here α is the thermal diffusivity defined as λ/C. Equation (6) implies that the effect of a heat pulse is felt instantaneously throughout the domain. In other words, the heat waves travel with infinite speed. Under steady state a well-defined temperature gradient is established across the film and no temperature jump is predicted. The solution to this equation for the isothermal boundary conditions is

$$\theta=1-\xi-\frac{2}{\pi}\sum_{m=1}^{\infty}\frac{1}{m}\sin(m\pi\xi)\exp\left(-\frac{m^2\pi^2\tau}{3\eta_L}\right). \tag{8}$$

The boundary heat flux at $\xi=0$, nondimensionalized by $\sigma(T_1^4-T_0^4)$, is

$$Q=\beta\left[1+2\sum_{m=1}^{\infty}\exp\left(-\frac{m^2\pi^2\tau}{3\eta_L}\right)\right], \tag{9}$$

where $\beta=[\lambda(T_1-T_0)/L\sigma(T_1^4-T_0^4)]$. Equation (9) suggests that for $\tau\to 0$ the heat flux Q tends to infinity.

B. Hyperbolic heat equation

The hyperbolic heat equation (HHE) can be obtained by combining Eq. (4) with the energy balance equation

$$\frac{\partial e}{\partial t}=-\nabla\cdot\mathbf{q}, \tag{10}$$

where $\partial e/\partial t$ is the rate of change in internal energy which can be written as

$$\frac{\partial e}{\partial t}=C\frac{\partial T}{\partial t}. \tag{11}$$

The resulting hyperbolic heat equation is

$$\tau_R\frac{\partial^2 T}{\partial t^2}+\frac{\partial T}{\partial t}=\alpha\frac{\partial^2 T}{\partial x^2}, \tag{12}$$

with boundary conditions

$$\text{at } t=0,\ T=T_0,\ \frac{\partial T}{\partial t}=0,$$
$$\text{at } x=0,\ T=T_1,\quad \text{at } x=L,\ T=T_0. \tag{13}$$

This equation suggests that heat waves travel at a finite speed of $\sqrt{\alpha/\tau_R}$ although the amplitude decays exponentially with time. Under steady state, the HHE also gives a well-established temperature gradient with no temperature jumps at the boundaries. The solution to this equation is

$$\theta=1-\xi-\frac{e^{-\tau\eta_L/2}}{\pi}\sum_{m=1}^{\infty}\left[\left(\frac{1+\delta_m}{\delta_m}\right)\exp\left(\frac{\delta_m\eta_L\tau}{2}\right)+\left(\frac{-1+\delta_m}{\delta_m}\right)\exp\left(-\frac{\delta_m\eta_L\tau}{2}\right)\right]\sin(m\pi\xi), \tag{14}$$

and the dimensionless boundary heat flux at $\xi=0$ is given as

$$Q=\beta\left(e^{-\tau\eta_L}-1+2e^{-\tau\eta_L/2}\times\sum_{m=1}^{\infty}\frac{-\exp(\delta_m\tau\eta_L/2)+\exp(-\delta_m\tau\eta_L/2)}{\delta_m}\right), \tag{15}$$

where $\delta_m=\sqrt{1-(4m^2\pi^2/3\eta_L^2)}$. Note that since $\alpha=\lambda/C$ and $\lambda=\frac{1}{3}Cv^2\tau_R$, the heat wave speed is predicted to be $v/\sqrt{3}$. The factor $\sqrt{3}$ is present because the thermal conductivity predicted by kinetic theory assumes energy propagation in all three directions. This turns out to be incorrect in ballistic transport since the energy propagation speed is the speed of sound v.

C. Equation of phonon radiative transport

The equation of phonon radiative transport[8] was derived from the Boltzmann transport equation[4] for the case of one-dimensional heat transport by phonons between two parallel plates (shown in Fig. 2). The Boltzmann equation is given by

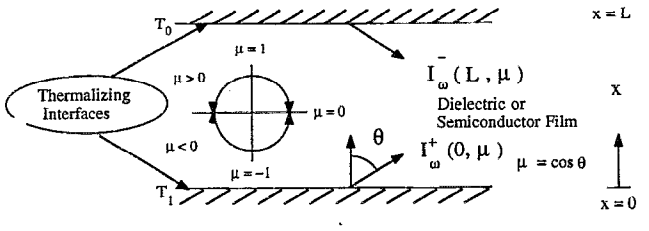

FIG. 2. Schematic diagram of a thin film of thickness L the boundaries of which are maintained at temperatures T_0 and T_1. The phonon intensities are also schematically represented.

$$\frac{\partial N_{\mathbf{q}}}{\partial t}+\mathbf{v}\cdot\nabla N_{\mathbf{q}}=\left(\frac{\partial N_{\mathbf{q}}}{\partial t}\right)_{\text{scat}}. \tag{16}$$

Here $N_{\mathbf{q}}$ is the distribution function of phonons of wave vector $\mathbf{q}$ and $\mathbf{v}$ is the velocity vector. The following simplifications were made to derive the EPRT: (i) scattering term approximated by relaxation time

$$(\partial N_{\mathbf{q}}/\partial t)_{\text{scat}}=(N_{\mathbf{q}}^0-N_{\mathbf{q}})/\tau_R(\mathbf{q});$$

(ii) define phonon intensity analogous to that of photons as the energy flow per unit time, per unit area, per solid angle in the direction of phonon propagation, and per unit frequency interval around ω given by[6]

$$I_\omega(\theta,\phi,x,t)=\sum_p v_p(\theta,\phi)N_{\mathbf{q}}(x,t)\hbar\omega_p(\mathbf{q})\mathscr{D}(\omega), \tag{17}$$

where $\hbar\omega(\mathbf{q})$ is the quantum of phonon energy of frequency $\omega(\mathbf{q})$ and $\mathscr{D}(\omega)$ is the density of states. Here θ is the polar angle and ϕ is the azimuthal angle as shown in the coordinate system in Fig. 3 and the summation is over the phonon polarizations p. By multiplying Eq. (16) by $v\hbar\omega(\mathbf{q})\mathscr{D}(\omega)$ and using the definition of intensity from Eq. (17), the resulting EPRT for intensity in the direction x is

$$\frac{1}{v}\frac{\partial I_\omega}{\partial t}+\mu\frac{\partial I_\omega}{\partial x}=\frac{I_\omega^0[T(x)]-I_\omega}{v\tau_R(\omega,T)}, \tag{18}$$

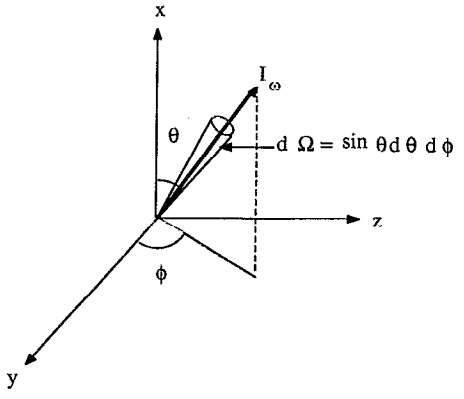

FIG. 3. Schematic diagram of the coordinate system showing the phonon intensity and the various angles.

where $\mu=\cos\theta$. Note that the local equilibrium intensity distribution I_ω^0 is a function of temperature only which in turn depends on the location x. The heat flux at any point can then be defined as

$$q=\sum_p \sum_q v_p(\theta,\phi)N_q(x,t)\hbar\omega(q)\mathscr{D}(\omega)$$
$$=\int_{\Omega=4\pi}\int_0^{\omega_D}\mu I_\omega(x,\omega,\Omega)d\omega\, d\Omega, \tag{19}$$

where $d\Omega$ is the incremental solid angle shown in Fig. 3. In terms of θ and ϕ the incremental solid angle is $d\Omega=\sin\theta\, d\theta\, d\phi$. If the phonon intensity is assumed to be independent of the azimuthal angle ϕ, then the heat flux can be written as

$$q=2\pi\int_{-1}^{1}\int_0^{\omega_D}\mu I_\omega(x,\omega,\Omega)d\omega\, d\mu. \tag{20}$$

If the EPRT in Eq. (18) is integrated over μ and ω in the range $-1<\mu<1$ and $0<\omega<\omega_D$ then the following equation is derived:

$$\frac{\partial e}{\partial t}+\nabla\cdot q=\int_0^{\omega_D}\int_{\mu=-1}^{1}\frac{I_\omega^0[T(x)]-I_\omega}{v\tau_R(\omega,T)}d\mu\, d\omega. \tag{21}$$

Under the first law of thermodynamics given in Eq. (10) it is clear that the right-hand side of Eq. (21) is equal to zero. Although Eq. (21) suggests that the integral over all frequencies is equal to zero, we simplify the calculations by invoking a more stringent condition of equality at every frequency,

$$I_\omega^0[T(x)]=\frac{1}{2}\int_{-1}^{1}I_\omega\, d\mu. \tag{22}$$

Substituting this in Eq. (18) one obtains

$$\frac{1}{v}\frac{\partial I_\omega}{\partial t}+\mu\frac{\partial I_\omega}{\partial x}=\frac{\frac{1}{2}\int_{-1}^{1}I_\omega\, d\mu-I_\omega}{v\tau_R(\omega,T)}. \tag{23}$$

This integro-differential equation is similar to the one used for photon radiative transfer.[9] To numerically solve this integro-differential form of the EPRT, it is convenient to separate the intensity I_ω into a forward component $I_\omega^+(x,\mu)$ and a backward component $I_\omega^-(x,\mu)$ depending on the sign of μ (see Fig. 2).[9] This results in the following equations, one each for I_ω^+ and I_ω^-, as

$$\frac{1}{v}\frac{\partial I_\omega^+}{\partial t}+\mu\frac{\partial I_\omega^+}{\partial x}=\frac{\frac{1}{2}\int_{-1}^{1}I_\omega\, d\mu-I_\omega^+}{v\tau_R(\omega,T)}\quad\text{for }\mu>0, \tag{24}$$

$$\frac{1}{v}\frac{\partial I_\omega^-}{\partial t}+\mu\frac{\partial I_\omega^-}{\partial x}=\frac{\frac{1}{2}\int_{-1}^{1}I_\omega\, d\mu-I_\omega^-}{v\tau_R(\omega,T)}\quad\text{for }\mu<0. \tag{25}$$

The boundary conditions can be written as

$$I_\omega^+(t,\mu,0)=I_\omega^0(T_1)\quad\text{for }\mu>0, \tag{26}$$

$$I_\omega^-(t,\mu,1)=I_\omega^0(T_0)\quad\text{for }\mu<0, \tag{27}$$

where $I_\omega^0(T_1)$ and $I_\omega^0(T_0)$ are the equilibrium intensities corresponding to temperatures T_1 and T_0, respectively. Once the intensity is evaluated from Eqs. (24) and (25) as a function of time, position, and frequency, the heat flux can be calculated from Eq. (20) as

$$q(x,t)=2\pi\left(\int_{\mu=-1}^{0}\int_0^{\omega_D}\mu I_\omega^-(x,\omega,\mu)d\omega\, d\mu+\int_{\mu=0}^{1}\int_0^{\omega_D}\mu I_\omega^+(x,\omega,\mu)d\omega\, d\mu\right), \tag{28}$$

and the temperature can be calculated by the relation

$$\int_{\omega=0}^{\omega_D}\sum_p v_p\frac{\hbar\omega\mathscr{D}(\omega)}{\exp[\hbar\omega/k_BT(x)]-1}d\omega=\frac{1}{2}\int_{\omega=0}^{\omega_D}\int_{\mu=-1}^{1}I_\omega(x,\mu)d\mu\, d\omega. \tag{29}$$

Equation (29) uses the Bose–Einstein statistics as the equilibrium phonon distribution.[12]

It should be noted that Eqs. (24) and (25) are wave equations with speeds $v\mu$ which will produce intensity waves that are attenuated due to scattering represented by the right-hand side of the equations. These equations are solved using the explicit upstream differencing method, i.e., using backward differencing in space when the wave is traveling in the positive x direction [Eq. (24)] and using forward differencing in space when it is traveling in the negative x direction [Eq. (25)]. In both equations forward difference in time was used ensuring $\Delta t\leqslant\Delta x/(v|\mu|)$ to make it stable. The frequency range $(0<\omega<\omega_D)$ for ω was divided into 29 divisions and the range of cosine of the angle $(-1<\mu<1)$ was divided into 19 divisions. The grid size $\Delta\xi$ was chosen to be 0.025. These discretizations gave a numerical error of less than 1%.

III. APPLICATION TO DIAMOND THIN FILMS

The development of the transient EPRT has so far been general and can be applied to any material. Consider diamond as an example for applying the theory to demonstrate the heat transport characteristics at small time and spatial scales.

The physical constants of ^{12}C diamond are given in Table I. Since the Debye temperature $\theta_D=1860$ K, one can assume a Debye density of states at room temperature which is[14]

$$\mathscr{D}(\omega)=\omega^2/2\pi^2v^3,\quad 0<\omega<\omega_D, \tag{30}$$

where ω_D is the cutoff frequency. The effective relaxation time $\tau_R(\omega,T)$ can be calculated using the Matthiessen rule[4] as

$$1/\tau_R=(1/\tau_i)+(1/\tau_U), \tag{31}$$

where τ_i and τ_U are the relaxation times for impurity and Umklapp scattering, respectively. Although normal processes or N scattering are important at intermediate temperatures[15] we have neglected them for the sake of simplicity.

Note that we have included only bulk scattering processes and not boundary scattering as is commonly used

TABLE I. Physical properties of type-IIa diamond.

Lattice constant a	3.57 Å[a]
Specific heat C	517.05 [J/kg K][b] at 300 K
Mass density ρ	3510 kg/m^3 [b]
Debye temperature θ_D	1860 K[a]
Speed of sound v	12 288 m/s
Constant A in Eq. (36)	163.94[c]
Stefan–Boltzmann constant σ	50.47 [W/m^2 K^4][c]

[a]Ashcroft and Mermin (see Ref. 12).
[b]Touloukian and Buyco (see Ref. 13).
[c]See explanation in text.

for the effective relaxation time. Instead, we defined an acoustical thickness η_L of the medium in Sec. II as

$$\eta_L = L/v\tau_R = L/l, \tag{32}$$

similar to the optical thickness defined in photon radiative transfer.[9] One must note that the mean free path is a statistical quantity such that the probability p that a particle can transverse a distance x without scattering is $p \sim \exp(-x/l)$.[16] Therefore, when $\eta_L = L/l \to 0$, the probability of no scattering event is $p \to 1$. Then the transport is purely ballistic and the medium can be called acoustically thin. If boundary scattering is included in Eq. (31) then the largest value of η_L would be unity for which the probability $p=0.37$. Therefore the purely ballistic limit cannot be represented if the relaxation time for boundary scattering is included in Eq. (31). In this limit Majumdar[8] showed that the Casimir limit can be obtained from the EPRT. Under diffusive transport $\eta_L \to \infty$ and the medium is acoustically thick for which the EPRT produces the Fourier law.

The relaxation time τ_i for impurity scattering can be approximated as

$$\tau_i = 1/\alpha\varphi\eta v, \tag{33}$$

where α is a constant of the order of unity, η is the number of scattering sites per unit volume or defect density, and φ, the scattering cross section, is assumed to vary as[8]

$$\varphi = \pi R^2[\chi^4/(\chi^4+1)]. \tag{34}$$

In the above equation, R is the radius of the lattice imperfection and χ is the size parameter defined as

$$\chi = 2\pi R/\Lambda = \omega R/v, \tag{35}$$

and Λ is the phonon wavelength. The assumed scattering cross section in Eq. (34) has correct limiting behaviors of Rayleigh law in the large-wavelength range and projected area of the defect in the small-wavelength regime, and involves a smooth transition between them.[17] The Umklapp relaxation time τ_U is approximated as[18]

$$\tau_U = A(T/\theta_D\omega)\exp(\theta_D/\gamma T), \tag{36}$$

where A is a nondimensional constant which depends on the atomic mass, the lattice spacing, and the Gruinessen constant[12] and γ is a parameter representing the effect of crystal structure. This relation predicts the thermal conductivity to vary as $\lambda \sim T^3 \exp(\theta_D/\gamma T)$ which has been observed experimentally for several materials.[4] The value of A has been calculated by Majumdar[8] and is given in Table I. The room-temperature thermal conductivities of type-IIa diamond with different concentrations of ^{13}C isotropic impurity were measured by Anthony *et al.*[19] and are listed in Table II. Using Eq. (2) for thermal conductivity, we calculated the effective mean free path. Using the relations for τ_i and τ_U and the Matthiessen rule we separated the contributions of impurity scattering and Umklapp scattering and listed them in Table II. The phonon frequency used for the calculations is that dominant in energy. This is calculated from the relation $\hbar\omega_{\text{dom}} = k_B T$. It was encouraging to observe that the mean free path for Umklapp scattering is independent of the impurity concentration as expected.

IV. RESULTS

In this section results are presented for transient heat transport in thin diamond films of thicknesses 0.1, 1.0, and 10 μm, initially at a temperature of 300 K, when the temperature of one boundary of the film is suddenly increased by $\Delta T = 0.1$ K. From Table II, the mean free path of phonons under three different concentrations is calculated to be of the order of 1 μm. Therefore, for films of thickness of the order of 1 μm or less, macroscopic heat transport laws cannot be applied.[20] The relaxation time τ_R, in HHE was calculated as l/v where l is the effective mean free path and v is the speed of sound. From the values in Tables I and II, τ_R was calculated to be 36.5 ps for a 0.07% concentration of ^{13}C. This impurity concentration is used for all the calculations of heat transport.

Figure 4 shows the temperature profile in a diamond thin film of thickness $L=0.1$ μm at dimensionless times of $\tau=0.1$, $\tau=1.0$, and steady state. This film thickness is smaller than the mean free path and therefore partially ballistic heat transport is expected. At $\tau=0.1$, the Fourier

TABLE II. Thermal conductivities and mean free paths of type-IIa diamond at room temperature for different concentrations of ^{13}C isotope. MFP denotes mean free path.

Concentration of ^{13}C in %[a]	Number density $\eta \times 10^{-26}$ (m^{-3})	Thermal conductivity[a] λ (W/m K)	Effective mean free path, l (μm)	Predicted impurity MFP l_I (μm)	U-process mean free path l_U (μm)
0.07	0.154	3320	0.447	9.57	0.468
0.50	1.100	2600	0.350	1.34	0.473
1.00	2.200	2230	0.273	0.67	0.461

[a]Data from Anthony *et al.* (see Ref. 19).

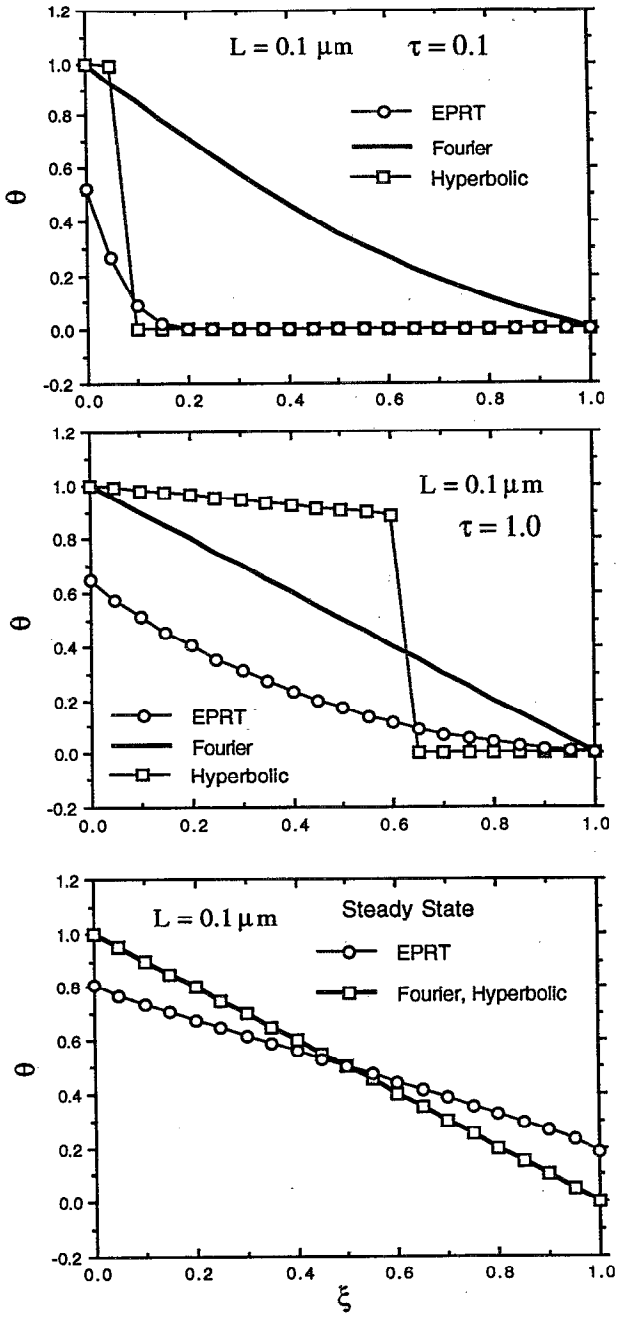

FIG. 4. Variation of dimensionless temperature profiles predicted by the EPRT, Fourier law, and hyperbolic heat equation as functions of dimensionless time for a diamond film of thickness 0.1 μm. Here $\theta=(T-T_0)/(T_1-T_0)$, $\tau=t/(l/v)$ and $\xi=x/L$. The wave nature of hyperbolic heat equation and the ballistic transport in the form of temperature jumps at the boundaries predicted by EPRT is clearly seen. The Fourier law clearly overpredicts the rate of evolution of temperature profiles.

law predicts a well-established temperature profile within the film thickness. The HHE as expected predicts a temperature discontinuity traveling as an attenuating wave across the film thickness. The amplitude attenuates because of diffusion. The EPRT predicts a temperature rise at the boundary $\xi=0$, decaying due to diffusion to the initial temperature near $\xi=0.2$. Although the EPRT is also a wave equation, these diffusion effects are seen because the relaxation time $\tau_R(\omega)$ at some phonon frequencies is very short. These phonon modes relax and give rise to some degree of diffusion which are absent in the solutions of HHE which assumes only an effective τ_R. As dimensionless time increases to 1.0, the Fourier limit predicts a steady-state temperature profile. Note that if the phonon transport is purely ballistic, $\tau=1$ corresponds to the time it takes for the phonons emitted from one boundary to reach the other. The temperature discontinuity wave predicted by the HHE reaches only $\xi=0.6$ with very little amplitude decay. This is because the speed of heat wave propagation is $v/\sqrt{3}$ as discussed earlier in Sec. III. The EPRT predicts that the effect of the temperature increase at the boundary $\xi=0$, begins to affect the vicinity of $\xi=1.0$.

At steady state, it is clear that both the Fourier limit and HHE show the same linear temperature profile as can be seen from the solutions in Eqs. (8) and (14). Temperature jumps at the boundaries are not predicted by either of these methods. In contrast the EPRT predicts the temperature jumps that are observed in the Monte Carlo simulation of Klitsner *et al.*[7] Dimensionless temperature jumps of 0.2 at both the boundaries were calculated by the EPRT for a film thickness of 0.1 μm. The time to reach 99.99% of steady state was $\tau_{SS}=0.7$ for Fourier law, $\tau_{SS}=20$ for the HHE, and $\tau_{SS}=13.55$ for the EPRT. The response of the material to sudden changes in boundary conditions, predicted by the EPRT, is much slower than that of Fourier limit because heat waves travel at a finite speed. However it is faster compared to the HHE because the heat wave predicted by the HHE moves at a speed of $v/\sqrt{3}$ and continues to get reflected from both the boundaries. Since the thickness of the film is small compared to the mean free path, the heat wave has to undergo multiple reflections before its amplitude attenuates sufficiently and steady state is reached; hence, the response is slower. Phonon reflection is not observed in the EPRT because the boundaries are assumed to be thermalizing black boundaries and not reflecting boundaries.

Figure 5 shows the temperature profiles in a diamond film of thickness $L=1.0$ μm at dimensionless times of $\tau=0.1$, $\tau=1.0$, and steady state. This figure is qualitatively similar to Fig. 4. The Fourier law again predicts a well-established temperature profile within the film compared to both the HHE and the EPRT at all the times shown. The most obvious difference is that the HHE predicts the temperature wave to attenuate because of stronger diffusion effects. The time to reach 99.99% of steady state predicted by the Fourier law and HHE is $\tau_{SS}=7$ and by the EPRT is $\tau_{SS}=47.5$. The reason for a faster response by the HHE compared to the smaller-thickness case is that the amplitude decay is substantial due to more dominant diffusion effects arising from larger film thickness such that multiple reflections from the boundaries are negligible. The temperature jump predicted by the EPRT ($\sim$0.03) is also considerably less than for the case of smaller thickness.

Figure 6 shows the temperature profiles in a diamond film of thickness $L=10$ μm at dimensionless times of $\tau=1$, $\tau=10$, and steady state. The temperature profiles are quite

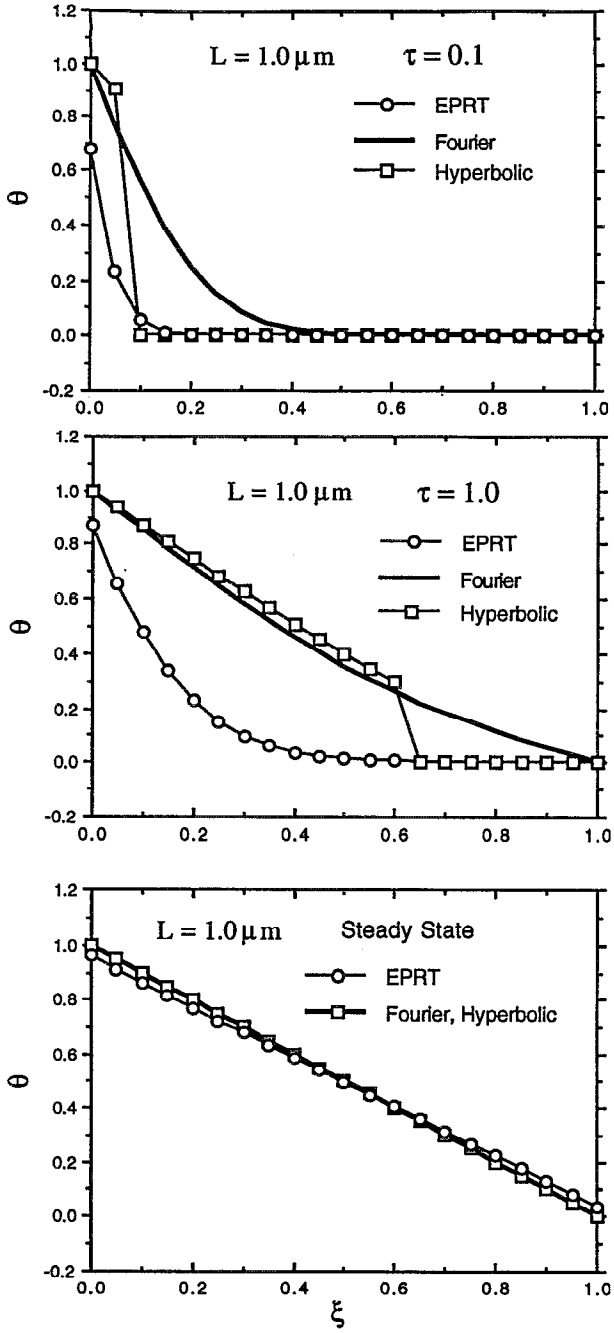

FIG. 5. Variation of dimensionless temperature profiles predicted by the EPRT, Fourier law, and hyperbolic heat equation as functions of dimensionless time for a diamond film of thickness 1 μm. The definitions of θ, τ, and ξ are as defined in Fig. 4. The wave nature of hyperbolic nature is decreased due to diffusion. Temperature jumps predicted by the EPRT are also much lower due to diffusion. The Fourier law again overpredicts the rate of evolution of the temperature profiles.

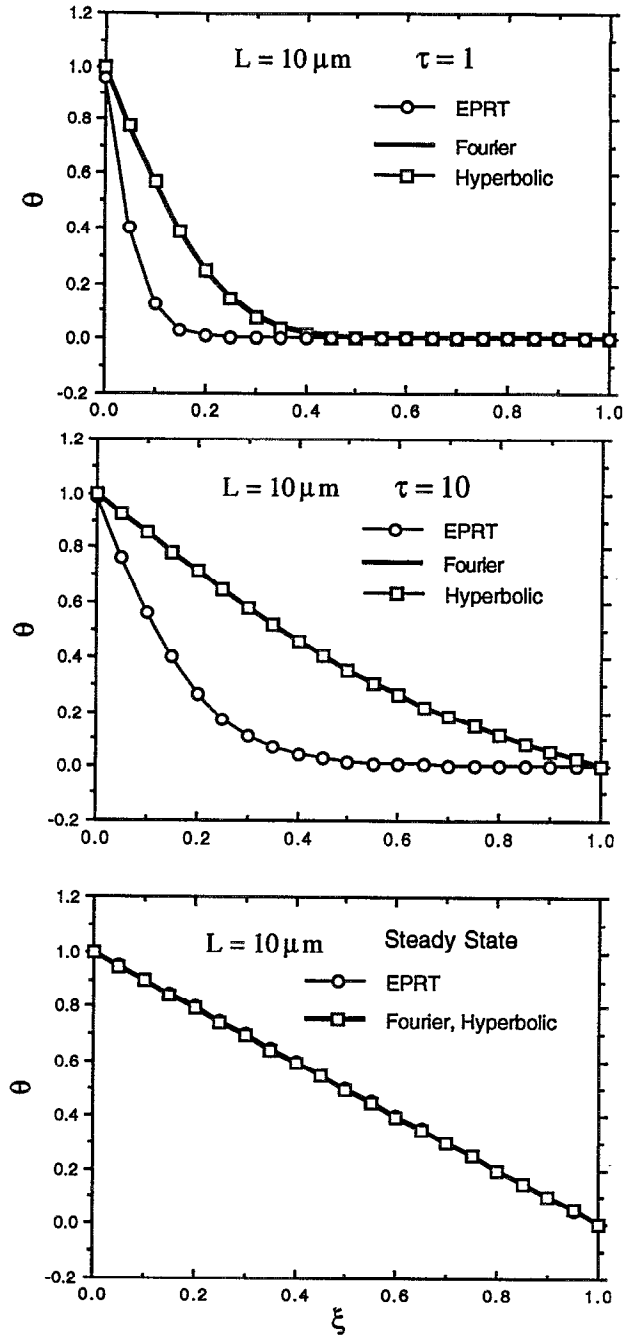

FIG. 6. Variation of dimensionless temperature profiles predicted by the EPRT, Fourier law, and hyperbolic heat equation as functions of dimensionless time for a diamond film of thickness 10 μm. The definitions of θ, τ, and ξ are as defined in Fig. 4. Diffusion effects are clearly evident. Here again the rates of evolution of temperature profiles predicted by the Fourier law and HHE are much higher compared to EPRT.

different from the cases discussed above. First, the Fourier limit and the HHE predictions match very closely. This is because the diffusion effects are much more dominant in the HHE causing the amplitude of the heat wave to decay substantially early on. The EPRT also predicts the same steady-state temperature profile with no temperature jumps due to dominant diffusion effects. The transient response, however, is markedly different at $\tau = 10$ even when diffusion is dominant. This can be critical in pulsed-laser processing of materials where the rate of temperature change determines the material microstructure.

Figure 7 shows the variation of the dimensionless boundary heat flux as a function of time for a film thickness of $L = 0.1$ μm. The Fourier law predicts a straight line corresponding to a summation of exponentially decaying

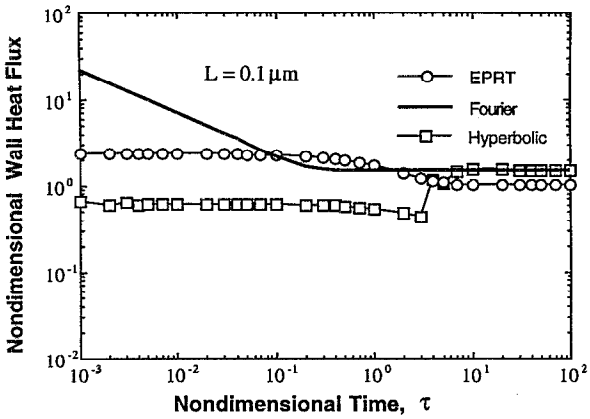

FIG. 7. Variation of dimensionless wall heat flux, $Q=q/\sigma(T_1^4-T_0^4)$, as a function of dimensionless time defined in Fig. 4 for a diamond film of thickness 0.1 μm. The Fourier law clearly overpredicts wall heat flux and the HHE underpredicts it as small time scales. At steady state both the classical laws overpredict the wall heat flux as has been demonstrated by Majumdar (see Ref. 8).

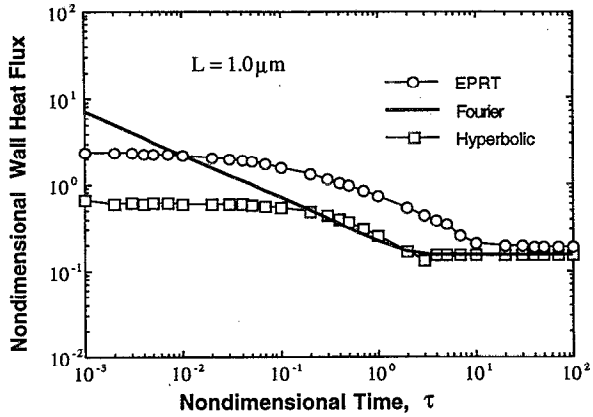

FIG. 8. Variation of dimensionless wall heat flux defined in Fig. 7 as a function of dimensionless time defined in Fig. 4 for a diamond film of thickness 1 μm. The Fourier law again clearly overpredicts wall heat flux and the HHE underpredicts it as small time scales. At steady state both the classical laws underpredict the wall heat flux slightly.

terms with respect to time shown in Eq. (8) until steady state is reached. The nondimensional boundary heat flux predicted by the EPRT remains constant at about 2 for $\tau<0.1$. During this period, the intensity wave emitted from one boundary does not reach the other boundary. Between $0.1<\tau<1$, the dimensionless boundary flux decreases due to diffusion and thermalization at the film surface. The boundary flux then reaches the steady state value of 1 at $\tau>1$ in accordance to the Casimir limit. The boundary heat flux predicted by the HHE, however, initially decays weakly with time, but later starts to oscillate while being decayed at the same time as can be seen in Eq. (15). This can be explained as follows. At small times, the temperature gradient at the wall is very small; therefore, when Eq. (9) is evaluated for the boundary heat flux, the right-hand-side term can be neglected, leading to an exponential decay with respect to time. As time increases the heat wave emerging at the boundary $\xi=0$ in the reflection of the wave which arrives at $\xi=0$ after reflecting from $\xi=1$ with a decayed amplitude. This leads to a higher-temperature gradient at the boundary and the boundary heat flux increases. These multiple reflections of the temperature wave cause oscillations in the boundary heat flux which eventually decay.

Figure 8 shows the variation of the dimensionless boundary heat flux as a function of time for a film of thickness 1.0 μm. This figure is similar to Fig. 7 qualitatively except for the results of HHE. In this figure, the heat flux decays at a higher rate for the HHE compared to Fig. 6 because of more dominant diffusion effects. In this case also the heat wave emerging at the boundary $\xi=0$, reflects off from the boundary $\xi=1$ and arrives at $\xi=0$ causing an increase in temperature gradient. However, here the heat wave has attenuated substantially and the increase in wall heat flux is not as much as in the previous case.

Figure 9 shows the boundary heat flux results for a film of thickness 10 μm. The HHE and the Fourier law predictions match exactly after dimensionless time of $\tau\sim1$. This is because the wavelike nature of the temperature discontinuity predicted by the HHE is dominant early on when the heat wave has not decayed substantially. The boundary heat flux predicted by the EPRT decays with time until it reaches steady state; however, under transient conditions, the flux predicted by the EPRT is more than that predicted by Fourier law. The reason is that since the transient response of the EPRT is slower than the Fourier law, the temperature gradient predicted by the EPRT is always more than that predicted by the Fourier law at any time before reaching steady state. Since in acoustically thick films the heat flux is proportional to the temperature gradient, a higher-temperature gradient implies a larger heat flux.

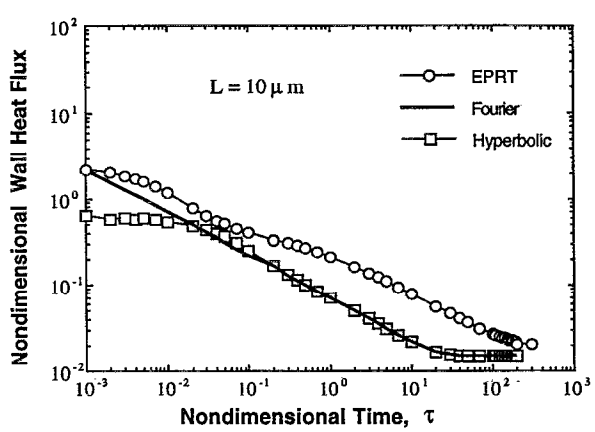

FIG. 9. Variation of dimensionless wall heat flux defined in Fig. 7 as a function of dimensionless time defined in Fig. 4 for a diamond film of thickness 10 μm. The HHE underpredicts the wall heat flux at small time scales. At steady state both the classical laws underpredict the wall heat flux slightly.

V. SUMMARY AND CONCLUSIONS

To analyze phonon heat transport under both short time and spatial scales, this study develops an equation of phonon radiative transfer (EPRT) similar to the one used for photons in thermal radiative transfer. This equation was used to study the transient thermal response of diamond thin films under ballistic and diffusive phonon transport. The results of the EPRT indicate a wavelike response for phonon intensity and temperature which under ballistic transport decays to a steady-state temperature profile with temperature jumps at the boundaries. The jumps are in accord with Monte Carlo simulations and are characteristic of ballistic phonon transport. Comparison of results with that of the Fourier law and the hyperbolic heat equation (HHE) suggest the following: (i) The Fourier law assumes diffusive transport and infinite wave speed and cannot be used for heat transport for short time and spatial scales; (ii) the HHE predicts the wavelike solution but not the temperature jumps under ballistic transport; therefore, the HHE could be used for transport under short time scales but not for short spatial scales; (iii) the EPRT can be used to study heat transport under both short time and spatial scales.

Under a sudden temperature jump at a film surface, the EPRT predicts that the surface heat flux could be as high as twice the steady-state Casimir limit for ballistic transport. The EPRT predictions also show that heat flux results can be significantly different from those predicted by the Fourier law and the HHE.

ACKNOWLEDGMENTS

The authors would like to thank M. Kulkarni (Arizona State University) for his help. This work was supported by the National Science Foundation. A. Majumdar gratefully acknowledges the support of NSF through the Young Investigator Award.

[1] S. M. Sze, *Physics of Semiconductor Devices*, 2nd ed. (Wiley, New York, 1981).
[2] W. W. Duley, *Laser Processing and Analysis of Materials* (Plenum, New York, 1983).
[3] W. Kurz and D. J. Fisher, *Fundamentals of Solidification* (Trans-Tech, Zürich, 1989).
[4] J. M. Ziman, *Electrons and Phonons* (Oxford University Press, London, 1960).
[5] H. B. G. Casimir, Physica **5**, 495 (1938).
[6] R. Siegel and J. R. Howell, *Thermal Radiation Heat Transfer*, 2nd ed. (Hemisphere, New York, 1982).
[7] T. Klitsner, J. E. VanCleve, H. E. Fischer, and R. O. Pohl, Phys. Rev. B **38**, 7576 (1988).
[8] A. Majumdar, J. Heat Transfer **115**, 7 (1993).
[9] M. N. Ozisik, *Radiative Transfer and Interactions with Conduction and Convection* (Wiley, New York, 1973).
[10] D. D. Joseph and L. Preziosi, Rev. Mod. Phys. **61**, 41 (1989).
[11] F. Claro and G. D. Mahan, J. Appl. Phys. **66**, 4213 (1989).
[12] N. W. Ashcroft and N. D. Mermin, *Solid State Physics* (Saunders, Philadelphia, 1976).
[13] Y. S. Touloukian and E. H. Buyco, *Thermophysical Properties of Matter* (IFI/Plenum, New York, 1970), Vol. 5.
[14] C. Kittel, *Introduction to Solid State Physics*, 6th ed. (Wiley, New York, 1986).
[15] J. Callaway, Phys. Rev. **113**, 1046 (1959).
[16] J. H. Jeans, *The Dynamical Theory of Gases*, 4th ed. (Dover, New York, 1954), p. 257.
[17] D. Walton and E. J. Lee, Phys. Rev. **157**, 720 (1967).
[18] P. G. Klemens, in *Solid State Physics*, edited by F. Seitz and D. Turnbull (Academic, New York, 1958), Vol. 7, pp. 1–98.
[19] T. R. Anthony, W. F. Banholzer, J. F. Fleischer, L. Wei, P. K. Kuo, R. L. Thomas, and R. W. Pryor, Phys. Rev. B **42**, 1104 (1990).
[20] M. I. Flik and C. L. Tien, J. Heat Transfer **112**, 872 (1990).